JCTC Journal of Chemical Theory and Computation

Expressivity of Determinantal Ansatzes for Neural Network Wave Functions

Ni Zhan, William A. Wheeler, Gil Goldshlager, Elif Ertekin, Ryan P. Adams, and Lucas K. Wagner*

Cite This: *J. Chem. Theory Comput.* 2025, 21, 9612−9619

Read Online

ACCESS | Metrics & More | Article Recommendations | Supporting Information

ABSTRACT: Neural network wave functions have shown promise as a way to achieve high accuracy in solving the many-body quantum problem. These wave functions most commonly use a determinant or a sum of determinants to antisymmetrize many-body orbitals, which are described by a neural network. In many cases, the wave function is projected onto a fixed-spin state. Such a treatment is allowed for spin-independent operators; however, it cannot be applied to spin-dependent problems, such as Hamiltonians containing spin−orbit interactions. We show that for spin-independent Hamiltonians, a strict upper bound property is obeyed between a traditional Hartree−Fock-like determinant, full spinor wave function, the full determinant wave function, and a generalized spinor wave function. The relationship between a spinor wave function and the full determinant arises because the full determinant wave function is the spinor wave function projected onto a fixed-spin, after which antisymmetry is implicitly restored in the spin-independent case. For spin-dependent Hamiltonians, the full determinant wave function is not applicable, because it is not antisymmetric. Numerical experiments on the H_3 molecule and two-dimensional homogeneous electron gas confirm these bounds.

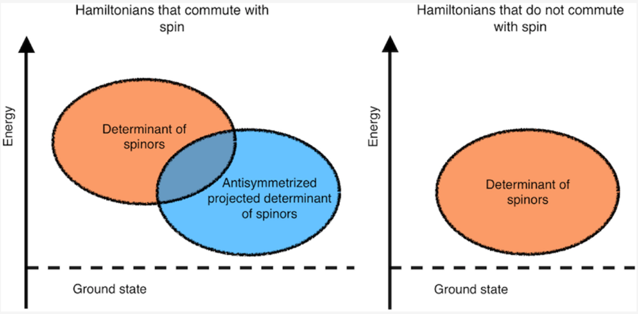

1. INTRODUCTION

Accurately computing the properties of many-electron systems is a central challenge in quantum chemistry, quantum physics, and materials science.[1,2] *Ab initio* descriptions of strongly correlated matter enable physical insights and understanding of materials exhibiting complex spin textures, superconductivity, superfluidity, and other exotic phases.[3,4] While modeling of many systems assumes spin-independent Hamiltonians, spin-dependent Hamiltonians are important for effects such as magnetism and spin−orbit coupling. High accuracy many-body calculations of spin-dependent Hamiltonians would elucidate new phenomena with applications to materials such as twisted bilayer graphene and transition metal dichalcogenides.

Many-body quantum calculations are challenging, because the Hilbert space of the wave function grows exponentially with increasing system size. The expressivity of the ansatz determines how closely a state in the Hilbert space (e.g., the ground state of the Hamiltonian) can be represented; thus, increasing expressivity achieves more accurate ground states, though at higher computational cost. Recent work has shown that a single determinant with infinitely flexible many-body orbitals completely represents any antisymmetric function.[5] Ansatzes using neural networks (NNs) to parametrize the many-body orbitals, trained with variational Monte Carlo, have reached state-of-the-art results because of their high degree of flexibility.[5−20] In practice, solution convergence is not quick, and a sum of determinants and the "full determinant" are used to increase variational freedom. Many NN wave functions trained in the first quantization project onto a fixed-spin configuration. Despite the relevance of spin-dependent interacting Hamiltonians, there has been less work on these.[21−24] The spin contamination of different Slater-Jastrow wave functions was investigated in Huang et al.[25] Recently, spin-dependent neural wave functions have been used for ultracold Fermi gases[26] nuclear physics[27] and fractional electron fillings in a Moiré material[28] and spin-based penalties in the training loss function have been used in Li et al.,[29] Szabó et al.[30]

Early NN wave functions used a generalization of the unrestricted Hartree−Fock ansatz to many-body orbitals, which we call *collinear* in this article.[5,7,9] Further work extended this ansatz to the full determinant[5,31] and spin-dependent spinor wave functions.[26] Given that the collinear and full determinant are projected onto a fixed-spin and that the orbitals of these ansatzes depend on spin differently, a natural question is the relation and generality between the ansatzes. In particular, the full determinant is widely used in

Received: July 28, 2025
Revised: September 10, 2025
Accepted: September 11, 2025
Published: September 17, 2025

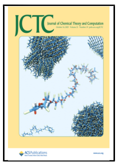

https://doi.org/10.1021/acs.jctc.5c01243

state-of-the-art NN wave functions, and its relation to other quantum chemistry ansatzes has been an open question.[32] Our paper provides a theoretical explanation.

We demonstrate that if the Hamiltonian and the many-body orbitals are spin-independent and otherwise identical, then the minimum energy NN ansatzes can be energetically ordered as follows: $E[\text{collinear}] \geq E[\text{spinor}] \geq E[P_S \text{ spinor}] = E[\text{fulldet}]$, where P_S is a projection onto a fixed-spin state. If the many-body orbitals are spin-dependent, which we call "generalized spinor", then we show further that $E[\text{fulldet}] \geq E[\text{gen spinor}]$. For spin-dependent Hamiltonians, the fulldet wave function cannot be used since it relies on spin projection. We show numerical experiments on model systems H_3 and two-dimensional homogeneous electron gas to confirm these results.

2. BACKGROUND

2.1. Many-Body Spinor Wave Function. The many-body orbital ϕ is a function $\mathbb{R}^{3n} \to \mathbb{C}$ of all n electron positions $R_i := \{r_i; \{r_j \backslash_i\}\}$ where $\{r_j \backslash_i\}$ indicates all electron positions except the i-th electron (the special particle), and the orbital value is invariant to permutation order of the $\{j \setminus i\}$ electrons. We use R to represent all of the electron positions.

The many-body spin–orbital maps from $\mathbb{R}^{3n} \to \mathbb{C}^2$

$$\langle R_i|\phi\rangle = \begin{pmatrix} \phi_\uparrow(R_i) \\ \phi_\downarrow(R_i) \end{pmatrix} \tag{1}$$

which may also be written as $\phi_\uparrow(R_i)|\uparrow_\mathrm{i}\rangle + \phi_\uparrow(R_i)|\downarrow_\mathrm{i}\rangle$. The spin–orbital is a two-component function for spin-1/2 particles, as it is the positional wave function tensored into the S_z eigenbasis for spin. Spin-1/2 particles have two S_z eigenstates, commonly called up $|\uparrow\rangle$ and down $|\downarrow\rangle$, and the spin state of an electron, s_i, can be represented as a normalized complex two-dimensional vector or superposition of the S_z eigenstates. The Hilbert space of the many-body spin–orbital is $\mathbb{L}^2(\mathbb{R}^{3n}) \otimes \mathbb{C}^2$.

The spinor determinant[33] is

$$\Psi_{\text{spinor}}(R, S) = \begin{vmatrix} s_1^\dagger \cdot \begin{pmatrix} \phi_{1,\uparrow}(R_1) \\ \phi_{1,\downarrow}(R_1) \end{pmatrix} & \cdots & s_n^\dagger \cdot \begin{pmatrix} \phi_{1,\uparrow}(R_n) \\ \phi_{1,\downarrow}(R_n) \end{pmatrix} \\ \vdots & \ddots & \vdots \\ s_1^\dagger \cdot \begin{pmatrix} \phi_{n,\uparrow}(R_1) \\ \phi_{n,\downarrow}(R_1) \end{pmatrix} & \cdots & s_n^\dagger \cdot \begin{pmatrix} \phi_{n,\uparrow}(R_n) \\ \phi_{n,\downarrow}(R_n) \end{pmatrix} \end{vmatrix} = \mathrm{Det}[\langle R_i, s_i|\phi_j\rangle] \tag{2}$$

where S is all of the electron spins. The spinor determinant is antisymmetric because an exchange of r_i, s_i and r_j, s_j only exchanges columns i and j, which results in a minus sign. The many-body orbitals of eq 2 depend on the positions of all particles but only on the spin of the i-th electron. We also describe a generalized version in which the orbitals include a permutation-invariant dependence of all spins in the next section.

2.2. Ansatzes. Commonly used quantum chemistry ansatzes are representable in the spinor form. A collinear ansatz contains spin–orbitals that are fully up or down; i.e., the spin–orbitals are all aligned along the same spin axis. The collinear determinant is

$$\langle R, S|\Psi_{\text{collinear}}\rangle = \begin{vmatrix} s_1^\dagger \cdot \begin{pmatrix} \phi_{1,\uparrow}(R_1) \\ 0 \end{pmatrix} & \cdots & s_n^\dagger \cdot \begin{pmatrix} \phi_{1,\uparrow}(R_n) \\ 0 \end{pmatrix} \\ \vdots & & \vdots \\ s_1^\dagger \cdot \begin{pmatrix} \phi_{n_\uparrow,\uparrow}(R_1) \\ 0 \end{pmatrix} & \cdots & s_n^\dagger \cdot \begin{pmatrix} \phi_{n_\uparrow,\uparrow}(R_n) \\ 0 \end{pmatrix} \\ s_1^\dagger \cdot \begin{pmatrix} 0 \\ \phi_{1,\downarrow}(R_1) \end{pmatrix} & \cdots & s_n^\dagger \cdot \begin{pmatrix} 0 \\ \phi_{1,\downarrow}(R_n) \end{pmatrix} \\ \vdots & & \vdots \\ s_1^\dagger \cdot \begin{pmatrix} 0 \\ \phi_{n_\downarrow,\downarrow}(R_1) \end{pmatrix} & \cdots & s_n^\dagger \cdot \begin{pmatrix} 0 \\ \phi_{n_\downarrow,\downarrow}(R_n) \end{pmatrix} \end{vmatrix} \tag{3}$$

where $n_\uparrow$ and $n_\downarrow$ represent the number of up and down orbitals, respectively. Note that the collinear ansatz is the only ansatz discussed here that requires selecting the number of up and down orbitals, which we index by $1, ..., n_\uparrow$ and $1, ..., n_\downarrow$. If we evaluate $\langle \uparrow \cdots \uparrow \downarrow \cdots \downarrow |\Psi_{\text{collinear}}\rangle$ with the number of spin-up and spin-down electrons the same as the number of up and down orbitals, the matrix is block diagonal with $\mathrm{Det}[\Psi] = \mathrm{Det}_\uparrow \mathrm{Det}_\downarrow$. For many systems, the lowest energy state is one with spins as half up and half down and the orbitals are chosen as $n_\uparrow = n_\downarrow = n/2$.

Restricted Hartree–Fock (RHF) is a special case of $\Psi_{\text{collinear}}$ with R_i replaced with r_i and $\phi_{i,\uparrow} = \phi_{i,\downarrow}$. The orbitals are single-particle orbitals, and spatial component of the up and down orbitals is the same. Unrestricted Hartree–Fock (UHF) is also a case of this ansatz with R_i replaced with r_i.

A noncollinear ansatz is one in which spin–orbitals are not constrained along a specified spin axis. The spinor determinant of eq 2 is a noncollinear ansatz, and Generalized Hartree–Fock (GHF) is a subset of spinor determinant with many-body orbitals replaced by single-body orbitals. It is clear that RHF ⊂ UHF ⊂ GHF, which implies the energy ordering $\min_{\Psi \in \text{RHF}} E[\Psi] \geq \min_{\Psi \in \text{UHF}} E[\Psi] \geq \min_{\Psi \in \text{GHF}} E[\Psi]$ by the variational principle. Similarly, $\min_{\Psi \in \text{collinear}} E[\Psi] \geq \min_{\Psi \in \text{spinor}} E[\Psi]$.

The full determinant ansatz was introduced in[5,31] to increase variational freedom. It has been used across several different NN wave functions including[7,10] and also referred to as dense determinant by.[20,34] The full determinant ansatz is formed from a precursor wave function as

$$\langle R, S|\Psi_{\text{precursor}}\rangle = \begin{vmatrix} s_1^\dagger \cdot \begin{pmatrix} \phi_{1,\uparrow}(R_1) \\ 0 \end{pmatrix} & \cdots & s_n^\dagger \cdot \begin{pmatrix} 0 \\ \phi_{1,\downarrow}(R_n) \end{pmatrix} \\ \vdots & \ddots & \vdots \\ s_1^\dagger \cdot \begin{pmatrix} \phi_{n,\uparrow}(R_1) \\ 0 \end{pmatrix} & \cdots & s_n^\dagger \cdot \begin{pmatrix} 0 \\ \phi_{n,\downarrow}(R_n) \end{pmatrix} \end{vmatrix} \tag{4}$$

The full determinant ansatz as defined in[5] is then $|\Psi_{\text{fulldet}}\rangle = |\uparrow \cdots \uparrow \downarrow \cdots \downarrow\rangle \langle \uparrow \cdots \uparrow \downarrow \cdots \downarrow |\Psi_{\text{precursor}}\rangle$, which produces a dense matrix of orbitals that is not block diagonal. Note that while collinear and spinor are antisymmetric, full determinant is not. The antisymmetry condition requires that the wave function gain a minus sign under exchange of both position and spin. Consider exchanging R_1, s_1 and R_n, s_n in eq 4. The original columns are of the form

$$s_1^\dagger \cdot \begin{pmatrix} \phi_{j,\uparrow}(R_1) \\ 0 \end{pmatrix} \text{and } s_n^\dagger \cdot \begin{pmatrix} 0 \\ \phi_{j,\downarrow}(R_n) \end{pmatrix}$$

while the new columns are of the form

$$s_n^\dagger \cdot \begin{pmatrix} \phi_{j,\uparrow}(R_n) \\ 0 \end{pmatrix} \text{and } s_1^\dagger \cdot \begin{pmatrix} 0 \\ \phi_{j,\downarrow}(R_1) \end{pmatrix}$$

not the same as exchanging the original columns and thereby not guaranteeing antisymmetry. However, for spin-independent operators, the expectation value of the antisymmetrized version of full determinant can be evaluated efficiently.

We introduce a generalized spinor which can describe both spinor and full determinant. The generalized spinor has been used in,[26−28]

$$\langle R, S|\Psi_g\rangle = \begin{vmatrix} s_1^\dagger \cdot \begin{pmatrix} \phi_{1,\uparrow}(R_1, \{S\}) \\ \phi_{1,\downarrow}(R_1, \{S\}) \end{pmatrix} & \cdots & s_n^\dagger \cdot \begin{pmatrix} \phi_{1,\uparrow}(R_n, \{S\}) \\ \phi_{1,\downarrow}(R_n, \{S\}) \end{pmatrix} \\ \vdots & \ddots & \vdots \\ s_1^\dagger \cdot \begin{pmatrix} \phi_{n,\uparrow}(R_1, \{S\}) \\ \phi_{n,\downarrow}(R_1, \{S\}) \end{pmatrix} & \cdots & s_n^\dagger \cdot \begin{pmatrix} \phi_{n,\uparrow}(R_n, \{S\}) \\ \phi_{n,\downarrow}(R_n, \{S\}) \end{pmatrix} \end{vmatrix} \tag{5}$$

where $\{S\}$ indicates a permutation-invariant dependence on S is included in every orbital. When using the overcomplete basis of electron spins as $s_i := \begin{bmatrix} a_i \\ b_i \end{bmatrix}$, $a_i^* a_i + b_i^* b_i = 1$, the wave function must satisfy $\langle s_i|\Psi\rangle = a_i^* \langle \uparrow_i |\Psi\rangle + b_i^* \langle \downarrow_i |\Psi\rangle$for all i, R, S. These constraints of linear superposition are easily satisfied for eq 5 in a discrete and complete basis for spin, e.g., $|\Psi = \frac{1}{\sqrt{2}}(|\uparrow\downarrow\rangle + |\downarrow\uparrow\rangle)$ for two electrons. However, an arbitrary spin configuration, such as $\langle s_1 s_2|\Psi\rangle$ where s_i are arbitrary spins on the Bloch sphere, requires the evaluation of an exponential number of coefficients, if eq 5 does not satisfy the linearity of spin superposition in the overcomplete basis directly. This results in a physically valid wave function but makes it exponentially expensive to evaluate the wave function at arbitrary superpositions of S, prohibiting the usage of the overcomplete basis in practice. This challenge also appeared in Kim et al.[26] Adams et al.[27] where they only sampled spins in the discrete basis, which can be inefficient for real space systems.

Figure 1 summarizes the relations between collinear, spinor, full determinant, and generalized spinor. Collinear is fully contained within full determinant, collinear ⊂ fulldet, since collinear must be block diagonal and full determinant need not be. However, the full determinant ansatz is not fully contained within spinor, because the spin−orbitals are not the same across all columns. Spinor is also not fully contained within full determinant since full determinant is always an eigenstate of S_z, while the spinor may or may not be. Therefore, the ordering of variational minima between spinor and full determinant is nonobvious. Generalized spinor contains spinor since choosing the orbitals that are independent of spin recovers the spinor determinant form. We will show that generalized spinor also contains full determinant in Section 3.4 and further discuss the validity of nonantisymmetric full determinant and energetic bounds in the remainder of the paper.

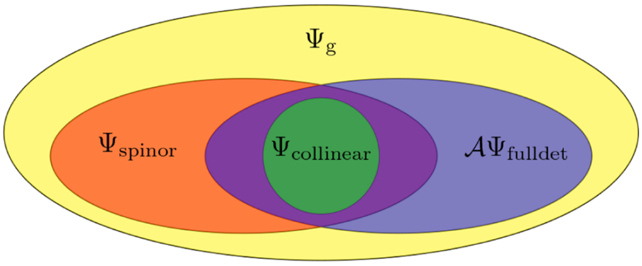

Figure 1. Containment relations of spinor determinant, antisymmetrized full determinant, collinear, and generalized spinor.

2.3. Spin Projection.

For a state in the spin and position the basis of $\mathbb{L}^2(\mathbb{R}^{3n}) \otimes \mathbb{C}^{2n}$, we use the notation

$$|R, S\rangle = |R\rangle|S\rangle \tag{6}$$

so that

$$\langle S|R, S\rangle = |R\rangle \tag{7}$$

$$\langle R|R, S\rangle = |S\rangle \tag{8}$$

The spin projection operator $P_S = |S\rangle\ \langle S\rangle$ projects a wave function onto the spin state $|S\rangle$. The result of a spin projection is a fixed-spin state, where each electron is projected to ↑ or ↓, e.g., $|\uparrow\downarrow\rangle\ \uparrow\downarrow|\Psi\rangle$. Another example of a fixed-spin state is the spinor wave function

$$\begin{vmatrix} \phi_{1,\uparrow}(R_1) & \phi_{1,\downarrow}(R_2) \\ \phi_{2,\uparrow}(R_1) & \phi_{2,\downarrow}(R_2) \end{vmatrix} |\uparrow\downarrow\rangle \tag{9}$$

A spin-projected wave function is not fully antisymmetric because it does not allow exchange of electrons with different spins. The full determinant as introduced in[5] is written for a fixed-spin state $|\uparrow \cdots \uparrow\downarrow \cdots \downarrow\rangle$ with $n_\uparrow$ up electrons and $n_\downarrow$ down electrons.

The correct resolution of the identity for computing expectation values is $\int dR\ \sum_S\ |R,S\rangle\ \langle R,S|$, which requires summing over all 2^n possible spin states. The sum over spin states is commonly omitted by projecting onto a fixed-spin state, which is valid when the antisymmetrized projected wave function has the same expectation as the spin-projected wave function. We show the exact statement and proof in the next section.

2.4. Evaluating Expectation Values of the Hamiltonian.

The expectation value of a general operator O (that may be spin-dependent and nonlocal) is

$$\langle\Psi|O|\Psi\rangle = \int dR dR' \sum_{S,S'} \langle\Psi|R, S\rangle\langle R, S|O|R', S'\rangle\langle R', S'|\Psi\rangle \tag{10}$$

where S and S' run over all configurations of the spins of all the electrons.

If O is independent of spin, it has the simplified expectation value

$$\langle R, S|O|R', S'\rangle = \delta_{SS'}\langle R|O|R'\rangle \tag{11}$$

removing the need to sum over secondary spin configurations. Applying this property to the expectation value in eq 10,

$$\langle\Psi|O|\Psi\rangle = \int dR dR' \sum_{S} \langle\Psi|R, S\rangle\langle R|O|R'\rangle\langle R', S|\Psi\rangle \tag{12}$$

The following theorem states that the spin-projected wave function has the same expectation as its antisymmetrized projected version for a spin-independent operator.[35]

Theorem 1. If Ψ can be written as an antisymmetrized fixed-spin wave function $\Psi = \mathcal{A}\Psi_S$ for some spin configuration S, then the expectation can be evaluated just from the projection onto S,

$$\langle \Psi | O | \Psi \rangle = \int dR dR' \langle \Psi_S | R \rangle \langle R | O | R' \rangle \langle R' | \Psi_S \rangle \tag{13}$$

proof. We summarize the proof which has been shown in Sec. IV.E of.[35] Consider the fixed-spin wave function Ψ_S having spin state S. Its antisymmetrized counterpart is a sum over permutations

$$\mathcal{A}\Psi_S = \frac{1}{n!} \sum_{\pi} (-1)^{\pi} P_{\pi} \Psi_S \tag{14}$$

The permutation P_π results in a new spin state S^π. Since $\langle S | S^\pi \rangle = 0$, each permutation π contributes a separate integral to the expectation value,

$$\langle \mathcal{A}\Psi_S | O | \mathcal{A}\Psi_S \rangle = \frac{1}{n!} \sum_{\pi} \int dR dR' \langle \Psi_{S^\pi} | R \rangle \langle R | O | R' \rangle \langle R' | \Psi_{S^\pi} \rangle \tag{15}$$

Note that the $(-1)\pi$ sign terms cancel out, so all contributions are positive. Since permuting integration variables changes nothing and Ψ_{S^π} is the same for all permutations, each term contributes $\langle \{ \Psi_S | O | \Psi_S \rangle$ up to a normalization factor, equal to the expectation value of the original Ψ_S.

The Hamiltonian is a semilocal operator (containing the differential operator for kinetic energy), meaning $\langle R | H\Psi \rangle$can be evaluated without the extra integral over R'. Combining this with spin independence of eq 12 yields the standard formulation

$$\langle \Psi | H | \Psi \rangle = \int dR \langle \Psi | R \rangle \langle R | H\Psi \rangle \tag{16}$$

which is independent of the spin details of Ψ (assuming a fixed total spin eigenstate). Hence, spin-projection is common and convenient for spin-independent Hamiltonians but generally invalid for spin-dependent Hamiltonians.

3. ANALYSIS

We will show that the full determinant wave function is equivalent to the projection of a spinor determinant onto a particular spin state. The spin-projected determinant gives the correct expectation value for a *spin-independent* Hamiltonian, but not for general *spin-dependent* Hamiltonians. We show this for two electrons and single-particle orbitals and the general case with many-electrons and many-body orbitals. We also establish that the full determinant (projected spinor) is a variational lower bound to the spinor for spin-independent Hamiltonians.

3.1. Two Electrons with Single-Particle Orbitals.

As a concrete example, we first consider a two-electron wave function composed of single-particle orbitals. We consider the general case of many-electrons and many-body orbitals in the next subsection.

The full determinant wave function for two electrons and single-particle orbitals is

$$|\Psi_{\text{fulldet}}\rangle = \begin{vmatrix} \phi_{1,\uparrow}(r_1) & \phi_{1,\downarrow}(r_2) \\ \phi_{2,\uparrow}(r_1) & \phi_{2,\downarrow}(r_2) \end{vmatrix} |\uparrow\downarrow\rangle \tag{17}$$

As mentioned in Section 2.2, this wave function is not fully antisymmetric because the orbital functions are different across the columns. We also note this wave function is a projection of the spinor determinant onto the $|\uparrow\downarrow\rangle$ spin state. Using the antisymmetrizer $\mathcal{A} = \frac{1}{n!} \sum_{\pi} (-1)^{\pi} P_{\pi}$, where π represents permutations and P_π represents permutation operator (permuting both positions and spins), the full determinant is antisymmetrized to

$$\begin{aligned} \mathcal{A}\Psi_{\text{fulldet}} &= \Psi_{\text{fulldet},\uparrow\downarrow} - \Psi_{\text{fulldet},\downarrow\uparrow} \\ &= \begin{vmatrix} \phi_{1,\uparrow}(r_1) & \phi_{1,\downarrow}(r_2) \\ \phi_{2,\uparrow}(r_1) & \phi_{2,\downarrow}(r_2) \end{vmatrix} |\uparrow\downarrow\rangle - \begin{vmatrix} \phi_{1,\uparrow}(r_2) & \phi_{1,\downarrow}(r_1) \\ \phi_{2,\uparrow}(r_2) & \phi_{2,\downarrow}(r_1) \end{vmatrix} |\downarrow\uparrow\rangle \end{aligned} \tag{18}$$

up to normalization.

Now we will show $\langle \mathcal{A}\Psi_{\text{fulldet}} | H | \mathcal{A}\Psi_{\text{fulldet}} \rangle = \langle \Psi_{\text{fulldet}} | H | \Psi_{\text{fulldet}} \rangle$. Assuming that H is spin-independent eq 11 and semilocal, the expectation of eq 10 can be simplified to

$$\int dR \sum_{S} \langle \Psi | R, S \rangle \langle R, S | H\Psi \rangle \tag{19}$$

For $\mathcal{A}\Psi_{\text{fulldet}}$, eq 19 simplifies to

$$\begin{aligned} &\frac{1}{2} \int dr_1 dr_2 \Psi^*_{\text{fulldet},\uparrow\downarrow}(r_1, r_2) [H\Psi_{\text{fulldet},\uparrow\downarrow}](r_1, r_2) \\ &\quad + \frac{1}{2} \int dr_1 dr_2 \Psi^*_{\text{fulldet},\downarrow\uparrow}(r_2, r_1) [H\Psi_{\text{fulldet},\downarrow\uparrow}](r_2, r_1) \end{aligned} \tag{20}$$

The first term is the same as the original full determinant eq 17, and the second term is equivalent by exchanging the integration variables r_1 and r_2. This shows that Ψ_{fulldet} has the same energy expectation as $\mathcal{A}\Psi_{\text{fulldet}}$.

eq 18 is a multideterminant wave function. Since it is the antisymmetrized projected spinor determinant and has the same expectation as the full determinant for spin-independent operators, the full determinant has multideterminant character. In the next two sections, we will show that this finding holds for many-electrons and many-body orbitals and that the antisymmetrized projected spinor wave function has a lower minimum energy expectation compared to the spinor wave function.

3.2. Full Determinant is Spin-Projected Spinor.

3.2 Now we show that $|\Psi_{\text{fulldet, }S}\rangle \propto P_S \, |\Psi_{\text{spinor}}\rangle$. For each determinant entry,

$$s_i \cdot \phi_j(R_i) = \phi_{j,\uparrow}(R_i) \langle s_i | \uparrow_j \rangle + \phi_{j,\downarrow}(R_i) \langle s_i | \downarrow_j \rangle \tag{21}$$

Clearly only the term matching the spin s_i is nonzero, resulting in the determinant

$$\begin{aligned} \langle R, S | \Psi_{\text{spinor}} \rangle &= \begin{vmatrix} \phi_{1,\uparrow}(R_1) & \cdots & \phi_{1,\downarrow}(R_{n_\uparrow+1}) & \cdots \\ \cdots & \cdots & \cdots & \cdots \\ \phi_{n,\uparrow}(R_1) & \cdots & \phi_{n,\downarrow}(R_{n_\uparrow+1}) & \cdots \end{vmatrix} \\ &= \langle R, S | \Psi_{\text{fulldet},S} \rangle \end{aligned} \tag{22}$$

This projected wave function may no longer be normalized. For projection onto a fixed-spin configuration S, the normalization factor is

$$w_S = \frac{\int dR |\langle R, S | \Psi_{\text{spinor}} \rangle|^2}{\sum_{S'} \int dR |\langle R, S' | \Psi_{\text{spinor}} \rangle|^2} \tag{23}$$

making the normalized wave function

$$|\Psi_{\mathrm{fulldet},S}\rangle = \frac{1}{\sqrt{w_S}} P_S |\Psi_{\mathrm{spinor}}\rangle \tag{24}$$

Note that w_S is always positive and $\sum_S w_S = 1$.

We have shown that the full determinant is a spin-projected spinor. By Theorem 1, the full determinant has the same expectation as its antisymmetrized version for a spin-independent operator. The antisymmetrized full determinant is not the same as the spinor determinant. From the definition of the antisymmetrizer $\mathcal{A}$, the antisymmetrized spin-projected spinor $\mathcal{A}|\Psi_{\mathrm{fulldet},S}\rangle$ is a multideterminant wave function with up to $n!$ determinants, in contrast to the single determinant $|\Psi_{\mathrm{spinor}}\rangle$.

3.3. Full Determinant Is Lower Bound to Spinor Determinant Energy for Spin-Independent Hamiltonians. We show that the expectation value of spinor determinant energy is an upper bound to the full determinant energy expectation for a spin-independent Hamiltonian.

Theorem 2. If H operates as the identity in the spin space (i.e., H is spin-independent), then

$$\langle \Psi_{\mathrm{spinor}} | H | \Psi_{\mathrm{spinor}} \rangle \geq \langle \Psi_{\mathrm{fulldet}} | H | \Psi_{\mathrm{fulldet}} \rangle \tag{25}$$

proof

$$\begin{aligned}
\langle \Psi_{\mathrm{spinor}} | H | \Psi_{\mathrm{spinor}} \rangle &= \sum_{S,S'} \langle \Psi_{\mathrm{spinor}} | S \rangle \langle S | H | S' \rangle \langle S' | \Psi_{\mathrm{spinor}} \rangle \\
&= \sum_{S} \langle \Psi_{\mathrm{spinor}} | S \rangle H_S \langle S | \Psi_{\mathrm{spinor}} \rangle \\
&= \sum_{S} w_S \langle \Psi_{\mathrm{fulldet},S} | H_S | \Psi_{\mathrm{fulldet},S} \rangle \\
&\geq \min_S \langle \Psi_{\mathrm{fulldet},S} | H_S | \Psi_{\mathrm{fulldet},S} \rangle
\end{aligned} \tag{26}$$

where we have used $\langle S|H|S'' \rangle = \delta_{S,S'} H_S$ for spin-independent H, eq 24, and $w_S \geq 0$.

We emphasize that the bounds apply across the ansatzes for a fixed orbital expressivity.

3.4. Generalized Spinor Contains Spinor and Full Determinant. It is clear that the generalized spinor recovers the spinor by simply dropping the extra dependence on $\{S\}$ from the orbitals. The generalized spinor also generalizes the antisymmetrized full determinant:

Theorem 3. Consider the generalized spinor determinant Ψ_g with orbitals

$$\phi_{j,\alpha}(R_i, \{S\}) = \phi_{j,\alpha}(R_i) \mathbf{I}_{n_\uparrow, n_\downarrow}(S) \tag{27}$$

where $\alpha \in \uparrow, \downarrow$ and $\mathrm{I}n\uparrow, n\downarrow(S)$ is the indicator variable for the event that S contains exactly $n_\downarrow$ up-spins and $n_\downarrow$ down-spins. Then Ψ_g is equivalent to an antisymmetrized full determinant with orbitals $\phi_{j,\alpha}(R_i)$.

For the purpose of representing Ψ_{fulldet}, we only need to consider collinear spins to match $\phi_{j,\alpha}(R_i$ and $\phi_{j,\alpha}(R_i)\{S\})$. In addition to clarifying the relation between Ψ_g and Ψ_{fulldet}, this theorem indicates the following on the full determinant ansatz itself. First, the antisymmetrized full determinant can be represented as a single determinant wave function. Second, in the antisymmetrized full determinant, the spin-projection and antisymmetrization appear in the form of an indicator function for the desired spin configuration. This observation is an additional viewpoint to the fact that the full determinant is a spin-projected spinor.

proof. Let Ψ_g be the generalized spinor determinant with orbitals given by eq 27 and Ψ_f be the full determinant with orbitals $\phi_{j,\alpha}(R_i)$. Additionally, let $S_f = |\uparrow \cdots \uparrow \downarrow \cdots \downarrow\rangle$ be the spin state with $n_\uparrow$ up-spins followed by $n_\downarrow$ down-spins. We now verify the equivalence $\Psi_g = \mathcal{A}\Psi_f$ by checking all collinear spin-states S using three cases.

Case 1: when $S = S_f$ it holds

$$\langle R, S_f | \Psi_g \rangle = \langle R, S_f | \Psi_f \rangle = \langle R, S_f | \mathcal{A}\Psi_f \rangle \tag{28}$$

with the first equality holding since $\mathrm{I}n_\uparrow, n_\downarrow(S_f) = 1$ and the second equality holding since $\langle \{PR, PS_f \mid \Psi_f \rangle = 0$ when P is a permutation other than the identity.

Case 2: when $S = PS_f$ for some permutation P, the equivalence holds by permuting the input state, utilizing the previous case, and permuting it back:

$$\begin{aligned}
\langle R, PS_f | \Psi_g \rangle &= \mathrm{sgn}(P) \langle P^{-1}R, S_f | \Psi_g \rangle \\
&= \mathrm{sgn}(P) \langle P^{-1}R, S_f | \mathcal{A}\Psi_f \rangle \\
&= \langle R, PS_f | \mathcal{A}\Psi_f \rangle
\end{aligned} \tag{29}$$

Case 3: when $S \neq PS_f$ for any permutation P, it holds

$$\langle R, S | \Psi_g \rangle = \langle R, S | \mathcal{A}\Psi_f \rangle = 0 \tag{30}$$

We showed that the full determinant is both a projection of the spinor (in Section 3.2), and a specific instance of the generalized spinor. In many NN ansatzes, the many-body spin–orbital depends on the spin of all electrons in a permutationally invariant way, as described by generalized spinor. However, with a fixed-spin projection, the permutation invariant dependence becomes equivalent to a dependence on only the spin of the i-th electron, as in the spinor.

4. NUMERICAL EXPERIMENTS

We implement the spinor, projected spinor, and collinear ansatzes to test the energetic bounds for H_3 molecule and 2D homogeneous electron gas. The spinor and projected spinor ansatzes have nonzero spin–orbital components for up and down orbitals while the collinear ansatz has fully up or down spin–orbitals that are spatially unrestricted. For the spinor ansatz, we sample each electron's spin, as a normalized complex two-vector, in the Markov chain. Hence, the electrons are allowed to have any spin on the Bloch sphere, and we propose spin moves from a von Mises-Fisher proposal distribution[36] centered at each electron's current spin on the sphere. Discrete sampling of spin would suffice for the integration, but as an overcomplete representation, sampling spin on the Bloch sphere has the same expectation value and often results in faster mixing.[21,22] In the Markov chain, we alternate spin and position moves while keeping the other fixed. The generalized spinor is expensive to evaluate using continuous sampling, and since discrete sampling of spin is inefficient, we leave testing of that result to future work. Details of sampling and optimization are provided in the Supporting Information. Data to reproduce the numerical results are provided in.[37]

4.1. Bounds on Ansatz Energy for an H_3 Molecule. We provide numerical evidence of the bound $E[\mathrm{collinear}] \geq E[\mathrm{spinor}] \geq E[P_S\ \mathrm{spinor}]$ for H_3, and show that the energy differences decrease with increasing NN capacity. Figure 2 shows the minimum energy vs orbital expressivity for H_3 and the spinor, projected spinor, and collinear ansatzes. For this experiment, we simulated H_3 with open boundary conditions

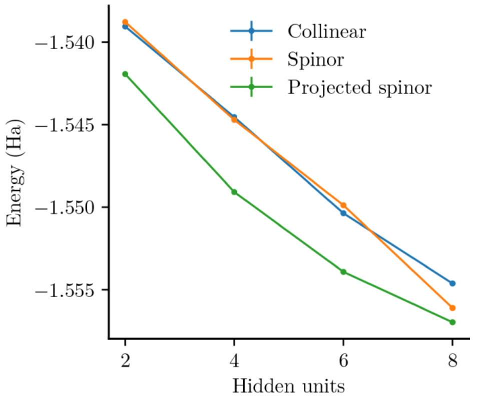

Figure 2. Numerical experiments showing the relationship between wave function ansatz on an equilateral triangle molecule H_3, with a bond length of 2.5 Bohr. At each given orbital expressivity, the energy relation $E[\text{collinear}] \geq E[\text{spinor}] \geq E[P_S \text{ spinor}]$ is satisfied for all optimized wave functions, and energy difference decreases as orbital expressivity increases.

and used the FermiNet architecture with single stream features only and two hidden layers with 2, 4, 6, and 8 hidden units per layer. We used these small NNs because energy differences between the three ansatzes diminish with increasing orbital expressivity and are unresolvable when double stream features are included for the H_3 system. In machine learning, it is well-known that small neural networks are prone to high variance in their local minima across independent optimizations.[38−42] To avoid bias from local minima, we trained five independent random seeds for each ansatz and ran a separate MCMC evaluation on the minimum energy wave function across the seeds for the reported energy. The batch size was 32,000, and optimizations were run for 40,000 iterations. Figure 2 shows that the projected spinor is a lower bound in energy to spinor and collinear, and that spinor is a lower bound to collinear, given a fixed orbital expressivity. Although in our numerical experiment, the collinear, spinor, and projected spinor seem to converge in energies, this could be specific to our case, and collinear could be higher energy than spinor in other systems.[43] Prior work also found that the collinear remained higher in energy than projected spinor for single determinants and certain systems, even in the large NN regime.[31]

4.2. Spin-Independent and Corresponding Spin-Dependent System.

We show the energetic bounds for a larger spin-independent system and the failure of spin projection for a corresponding spin-dependent system, using the 2D homogeneous electron gas (2DEG) with and without Rashba interaction. The Hamiltonian for the system is

$$H = \sum_{i=1}^{n} \frac{p_i^2}{2m} + \lambda \sum_{i=1}^{n} (p_i^y \sigma_i^x - p_i^x \sigma_i^y) + V_{\text{Coul}}(R) \tag{31}$$

where λ determines the strength of the spin−orbit coupling (Rashba) term. We simulate 10 electrons at $r_s = 5$, setting $\lambda = 0$ for the spin-independent case and $\lambda = 0.1$ for the spin-dependent case. We use the FermiNet architecture with single and double stream features, each with two hidden layers and 2, 3, 4, and 5 hidden units per layer. For the spin-independent case, we trained five independent random seeds for each ansatz and started two trainings of spinor and projected spinor from trained weights of a collinear optimization. For the spin-dependent case, we trained two independent random seeds for each ansatz. The reported energy is from the inference run of the minimum energy wave function across the runs, since we are interested in the lowest energy for the ansatzes. Although the spinor and projected spinor can achieve lower energies than the collinear in principle, a lower energy wave function is not necessarily easier to find during optimization, especially for this particular system, setup, and the small NNs used. The batch size was 2,048 and optimizations were run for 90,000 iterations.

Figure 3a shows the energy vs orbital expressivity for the collinear, spinor, and projected spinor ansatzes. The spin-independent case confirms the expected bound, and shows that the bound becomes equality for three or more hidden units. For two hidden units, we expect optimizing more seeds would achieve lower energies for collinear and spinor. Including double stream features in the network shows that the bound also holds for many-body orbitals and the increase in expressivity decreases the difference in bound more rapidly. For a spin-independent Hamiltonian, it is more convenient to use a spin-projected ansatz to decrease computation from spin sampling.

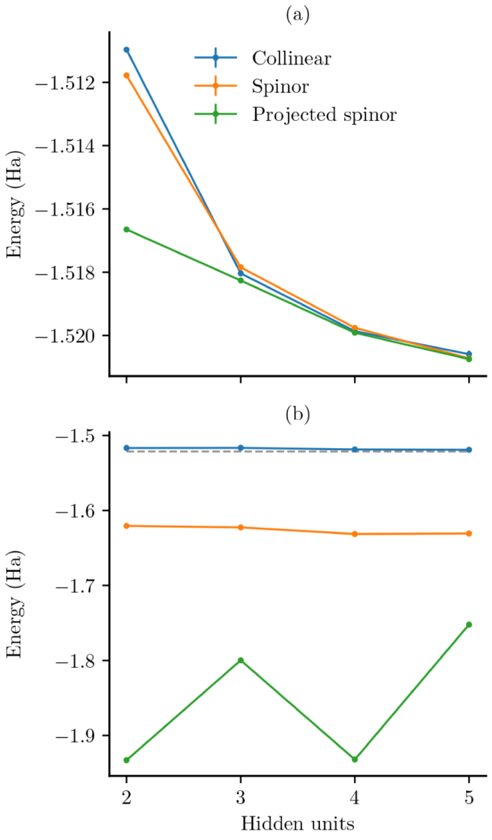

Figure 3. Numerical experiments on the periodic 2D homogeneous electron gas, with $r_s = 5$, for (a) spin-independent Hamiltonian and (b) spin-dependent Hamiltonian with a Rashba term, $\lambda = 0.1$. (a): At each given orbital expressivity, the energy relation $E[\text{collinear}] \geq E[\text{spinor}] \geq E[P_S \text{ spinor}]$ is satisfied in the spin-independent case. (b): In the spin-dependent case, collinear is unable to model spin effects, spinor correctly models spin effects, and projected spinor is nonvariational. Gray dashed line on spin-dependent plot indicates lowest energy from spin-independent plot.

Figure 3b shows that spin projection is incorrect for spin-dependent Hamiltonians. When the Rashba term is included, the collinear ansatz is unable to capture Rashba energy, and the projected spinor achieves a nonvariational energy. Both the collinear and projected spinor wave functions actually evaluate the wrong Hamiltonian: their expectation value is $\langle\Psi|H_S|\Psi\rangle$, where H_S is a partial projection of H onto an S subspace, whereas the evaluation for the spinor is $\langle\Psi|H|\Psi\rangle$, the correct expectation of the full Hamiltonian. The energy per electron achieved by the spinor ansatz (−0.163 Ha) is close to a reference of − 0.15775 Ha for the same system with 58 electrons in.[44] For spin-dependent Hamiltonians, the spinor determinant is a general ansatz that is variational and captures spin effects.

Demonstrating the bounds on a spin-independent system is a useful test to check the optimization and implementation. Best practices for optimizing NN wave functions is an active area of research[45] and NN wave functions have been found to achieve varying energies depending on the optimization settings.[34] In extending wave functions to spin-dependent systems, since the bound only applies to spin-independent systems, achieving the bound on a corresponding spin-independent system can be a useful first step and provide some information about implementation correctness.

5. CONCLUSIONS

We established a hierarchy of expressivity among the collinear, spinor, full determinant, and generalized spinor ansatzes. For spin-independent Hamiltonians and many-body orbitals that do not depend on spin, the minimum energies are ordered as $E[\text{collinear}] \geq E[\text{spinor}] \geq E[P_S\ \text{spinor}] = E[\text{fulldet}]$. If the many-body orbitals do depend on spin, then we obtain $E[\text{fulldet}] \geq E[\text{gen spinor}]$. We showed these relationships arise because the full determinant is a projection of spinor onto a fixed-spin state and also a specific instance of the generalized spinor. These results provide a new theoretical explanation for the commonly observed fact that full determinants are more expressive than collinear determinants in practice. We implemented the spinor NN wave function and confirmed the bounds for spin-independent Hamiltonians. Additionally, the spinor correctly captured spin-dependent energy, while full determinant is invalid since it relies on spin-projection. Our work opens the path to realistic simulation of both electron correlation and spin-dependent properties in materials.

■ ASSOCIATED CONTENT

Supporting Information

The Supporting Information is available free of charge at https://pubs.acs.org/doi/10.1021/acs.jctc.5c01243.

> Additional experiment details regarding neural network architecture, sampling, computation, and training, and additional validation experiments (PDF)

■ AUTHOR INFORMATION

Corresponding Author

Lucas K. Wagner − *AJL Institute for Condensed Matter Theory, Department of Physics, The Grainger College of Engineering, University of Illinois Urbana−Champaign, Urbana, Illinois 61801, United States;* orcid.org/0000-0002-3755-044X; Email: lkwagner@illinois.edu

Authors

Ni Zhan − *Department of Computer Science, Princeton University, Princeton, New Jersey 08544, United States;* orcid.org/0009-0002-3085-8780

William A. Wheeler − *Department of Electrical and Biomedical Engineering, University of Vermont, Burlington, Vermont 05405, United States*

Gil Goldshlager − *Department of Mathematics, University of California, Berkeley, Berkeley, California 94720, United States*

Elif Ertekin − *Department of Mechanical Science and Engineering, The Grainger College of Engineering, University of Illinois Urbana−Champaign, Urbana, Illinois 61801, United States;* orcid.org/0000-0002-7816-1803

Ryan P. Adams − *Department of Computer Science, Princeton University, Princeton, New Jersey 08544, United States*

Complete contact information is available at:
https://pubs.acs.org/10.1021/acs.jctc.5c01243

Notes

This report was prepared as an account of work sponsored by an agency of the United States Government. Neither the United States Government nor any agency thereof, nor any of their employees, makes any warranty, express or implied, or assumes any legal liability or responsibility for the accuracy, completeness, or usefulness of any information, apparatus, product, or process disclosed, or represents that its use would not infringe privately owned rights. Reference herein to any specific commercial product, process, or service by trade name, trademark, manufacturer, or otherwise does not necessarily constitute or imply its endorsement, recommendation, or favoring by the United States Government or any agency thereof. The views and opinions of authors expressed herein do not necessarily state or reflect those of the United States Government or any agency thereof.

The authors declare no competing financial interest.

■ ACKNOWLEDGMENTS

This work was partially supported by NSF OAC 2118201. N.Z. acknowledges support from the Princeton AI^2 initiative. G.G. acknowledges support from the U.S. Department of Energy, Office of Science, Office of Advanced Scientific Computing Research, Department of Energy Computational Science Graduate Fellowship under Award Number DE-SC0023112. The contributions of L.K.W. in supervising, writing, and creating the theory were supported by the U.S. Department of Energy, Office of Science, Office of Basic Energy Sciences, Computational Materials Sciences Program, under Award No. DE-SC0020177. The authors thank anonymous reviewers for their helpful comments and suggestions. This work used Princeton neuronic cluster and Delta GPU at the National Center for Supercomputing Applications through allocation MAT220011 from the Advanced Cyberinfrastructure Coordination Ecosystem: Services & Support (ACCESS) program, which is supported by National Science Foundation grants #2138259, #2138286, #2138307, #2137603, and #2138296.

■ REFERENCES

(1) Motta, M.; Genovese, C.; Ma, F.; Cui, Z.-H.; Sawaya, R.; Chan, G. K.-L.; Chepiga, N.; Helms, P.; Jiménez-Hoyos, C.; Millis, A. J.; Ray, U.; Ronca, E.; Shi, H.; Sorella, S.; Stoudenmire, E. M.; et al. Ground-State Properties of the Hydrogen Chain: Dimerization, Insulator-to-Metal Transition, and Magnetic Phases. *Phys. Rev. X* **2020**, *10*, 031058.

(2) Williams, K. T.; Yao, Y.; Li, J.; Chen, L.; Shi, H.; Motta, M.; Niu, C.; Ray, U.; Guo, S.; Anderson, R. J.; Li, J.; Tran, L. N.; Yeh, C.-N.; Mussard, B.; Sharma, S.; et al. Direct Comparison of Many-Body

Methods for Realistic Electronic Hamiltonians. *Phys. Rev. X* **2020**, *10*, 011041.

(3) Martin, R. M. *Electronic structure: Basic theory and practical methods*; Cambridge university press, 2020.

(4) Smith, J. C.; Burke, K. Interacting Electrons: Theory and Computational Approaches. *Am. J. Phys* **2017**, *85*, 636−637.

(5) Pfau, D.; Spencer, J. S.; Matthews, A. G. D. G.; Foulkes, W. M. C. Ab Initio Solution of the Many-Electron Schrödinger Equation With Deep Neural Networks. *Phys. Rev. Res* **2020**, *2*, 033429.

(6) Hermann, J.; Spencer, J.; Choo, K.; Mezzacapo, A.; Foulkes, W. M. C.; Pfau, D.; Carleo, G.; Noé, F. Ab Initio Quantum Chemistry With Neural-Network Wavefunctions. *Nat. Rev. Chem* **2023**, *7*, 692.

(7) Hermann, J.; Schätzle, Z.; Noé, F. Deep-Neural-Network Solution of the Electronic Schrödinger Equation. *Nat. Chem* **2020**, *12*, 891−897.

(8) Carleo, G.; Troyer, M. Solving the Quantum Many-Body Problem With Artificial Neural Networks. *Science* **2017**, *355*, 602−606.

(9) Luo, D.; Clark, B. K. Backflow Transformations Via Neural Networks for Quantum Many-Body Wave Functions. *Phys. Rev. Lett* **2019**, *122*, 226401.

(10) Li, X.; Li, Z.; Chen, J. Ab Initio Calculation of Real Solids Via Neural Network Ansatz. *Nat. Commun* **2022**, *13*, 7895.

(11) Wilson, M.; Moroni, S.; Holzmann, M.; Gao, N.; Wudarski, F.; Vegge, T.; Bhowmik, A. Neural Network Ansatz for Periodic Wave Functions and the Homogeneous Electron Gas. *Phys. Rev. B* **2023**, *107*, 235139.

(12) Cassella, G.; Sutterud, H.; Azadi, S.; Drummond, N. D.; Pfau, D.; Spencer, J. S.; Foulkes, W. M. C. Discovering Quantum Phase Transitions With Fermionic Neural Networks. *Phys. Rev. Lett* **2023**, *130*, 036401.

(13) Smith, C.; Chen, Y.; Levy, R.; Yang, Y.; Morales, M. A.; Zhang, S. Unified Variational Approach Description of Ground-State Phases of the Two-Dimensional Electron Gas. *Phys. Rev. Lett* **2024**, *133*, 266504.

(14) Yoshioka, N.; Mizukami, W.; Nori, F. Solving Quasiparticle Band Spectra of Real Solids Using Neural-Network Quantum States. *Commun. Phys* **2021**, *4*, 106.

(15) Scherbela, M.; Gerard, L.; Grohs, P. Towards a Transferable Fermionic Neural Wavefunction for Molecules. *Nat. Commun* **2024**, *15*, 120.

(16) Linteau, D.; Moroni, S.; Carleo, G.; Holzmann, M. Universal Neural Wave Functions for High-Pressure Hydrogen. *arXiv*. **2025**.

(17) Xie, H.; Li, Z.-H.; Wang, H.; Zhang, L.; Wang, L. Deep Variational Free Energy Approach To Dense Hydrogen. *Phys. Rev. Lett* **2023**, *131*, 126501.

(18) Pescia, G.; Nys, J.; Kim, J.; Lovato, A.; Carleo, G. Message-Passing Neural Quantum States for the Homogeneous Electron Gas. *Phys. Rev. B* **2024**, *110*, 035108.

(19) Scherbela, M.; Gao, N.; Grohs, P.; Günnemann, S. Accurate Ab-Initio Neural-Network Solutions To Large-Scale Electronic Structure Problems. *arXiv*. **2025**.

(20) Gerard, L.; Scherbela, M.; Marquetand, P.; Grohs, P. Gold-standard solutions to the Schrödinger equation using deep learning: How much physics do we need? *arXiv*. **2022**.

(21) Melton, C. A.; Bennett, M. C.; Mitas, L. Quantum Monte Carlo with variable spins. *J. Chem. Phys* **2016**, *144*, 244113.

(22) Melton, C. A.; Zhu, M.; Guo, S.; Ambrosetti, A.; Pederiva, F.; Mitas, L. Spin-orbit interactions in electronic structure quantum Monte Carlo methods. *Phys. Rev. A* **2016**, *93*, 042502.

(23) Schmidt, K.; Fantoni, S. A Quantum Monte Carlo Method for Nucleon Systems. *Phys. Lett. B* **1999**, *446*, 99−103.

(24) Lonardoni, D.; Gandolfi, S.; Lynn, J. E.; Petrie, C.; Carlson, J.; Schmidt, K. E.; Schwenk, A. Auxiliary Field Diffusion Monte Carlo Calculations of Light and Medium-Mass Nuclei With Local Chiral Interactions. *Phys. Rev. C* **2018**, *97*, 044318.

(25) Huang, C.-J.; Filippi, C.; Umrigar, C. J. Spin Contamination in Quantum Monte Carlo Wave Functions. *J. Chem. Phys* **1998**, *108*, 8838−8847.

(26) Kim, J.; Pescia, G.; Fore, B.; Nys, J.; Carleo, G.; Gandolfi, S.; Hjorth-Jensen, M.; Lovato, A. Neural-Network Quantum States for Ultra-Cold Fermi Gases. *Commun. Phys* **2024**, *7*, 148.

(27) Adams, C.; Carleo, G.; Lovato, A.; Rocco, N. Variational Monte Carlo Calculations of $A \leq 4$ Nuclei With an Artificial Neural-Network Correlator Ansatz. *Phys. Rev. Lett* **2021**, *127*, 022502.

(28) Luo, D.; Zaklama, T.; Fu, L. Solving Fractional Electron States in Twisted $MoTe_2$ With Deep Neural Network. *arXiv*. **2025**.

(29) Li, Z.; Lu, Z.; Li, R.; Wen, X.; Li, X.; Wang, L.; Chen, J.; Ren, W. Spin-Symmetry-Enforced Solution of the Many-Body Schrödinger Equation With a Deep Neural Network. *Nat. Comput. Sci* **2024**, *4*, 910−919.

(30) Szabó, P. B.; Schätzle, Z.; Entwistle, M. T.; Noé, F. An Improved Penalty-Based Excited-State Variational Monte Carlo Approach With Deep-Learning Ansatzes. *J. Chem. Theory Comput* **2024**, *20*, 7922−7935.

(31) Lin, J.; Goldshlager, G.; Lin, L. Explicitly Antisymmetrized Neural Network Layers for Variational Monte Carlo Simulation. *J. Comput. Biophys. Chem* **2023**, *474*, 111765.

(32) Schätzle, Z.; Szabó, P. B.; Mezera, M.; Hermann, J.; Noé, F. Deepqmc: An Open-Source Software Suite for Variational Optimization of Deep-Learning Molecular Wave Functions. *J. Chem. Phys* **2023**, *159*, 094108.

(33) Pauli, W. Zur Quantenmechanik Des Magnetischen Elektrons. *Zeitschrift für Phys* **1927**, *43*, 601−623.

(34) Von Glehn, I.; Spencer, J. S.; Pfau, D. A Self-Attention Ansatz for Ab-Initio Quantum Chemistry. *arXiv*. **2022**.

(35) Foulkes, W. M. C.; Mitas, L.; Needs, R. J.; Rajagopal, G. Quantum Monte Carlo Simulations of Solids. *Rev. Mod. Phys* **2001**, *73*, 33−83.

(36) Fisher, R. A. Dispersion on a sphere. *Proc. R. Soc. London, Ser. A* **1953**, *217*, 295−305.

(37) Zhan, N.; Wheeler, W. A.; Goldshlager, G.; Ertekin, E.; Adams, R. P.; Wagner, L. K. Data: Expressivity of determinantal anzatzes for neural network wave functions *arXiv*, **2025**.

(38) Frankle, J.; Carbin, M. The Lottery Ticket Hypothesis: Finding Sparse, Trainable Neural Networks. *arXiv* **2018**.

(39) Lawrence, S.; Giles, C. L.; Tsoi, A. C.Lessons in neural network training: Overfitting may be harder than expected*Proceedings of the Fourteenth National Conference on Artificial Intelligence*AAAI Press1997540−545

(40) Zou, D.; Gu, Q. An Improved Analysis of Training Over-parameterized Deep Neural Networks. *arXiv* **2019**.

(41) Allen-Zhu, Z.; Li, Y.; Song, Z.A Convergence Theory for Deep Learning via Over-Parameterization*Proceedings Of The 36th International Conference On Machine Learning*Proceedings of Machine Learning Research2019242−252

(42) Du, S.; Lee, J.; Li, H.; Wang, L.; Zhai, X.Gradient Descent Finds Global Minima of Deep Neural Networks*Proceedings Of The 36th International Conference On Machine Learning*Proceedings of Machine Learning Research20191675−1685

(43) Jiménez-Hoyos, C. A.; Rodríguez-Guzmán, R.; Scuseria, G. E. Polyradical Character and Spin Frustration in Fullerene Molecules: An Ab Initio Non-Collinear Hartree-Fock Study. *J. Phys. Chem. A* **2014**, *118*, 9925−9940.

(44) Ambrosetti, A.; Pederiva, F.; Lipparini, E.; Gandolfi, S. Quantum Monte Carlo Study of the Two-Dimensional Electron Gas in Presence of Rashba Interaction. *Phys. Rev. B* **2009**, *80*, 125306.

(45) Goldshlager, G.; Abrahamsen, N.; Lin, L. A Kaczmarz-Inspired Approach To Accelerate the Optimization of Neural Network Wavefunctions. *J. Comput. Biophys. Chem* **2024**, *516*, 113351.

https://doi.org/10.1021/acs.jctc.5c01243